JOURNAL OF APPLIED ELECTROCHEMISTRY **27** (1997) 916–927

Mathematical modelling of industrial aluminium cells with prebaked anodes
Part I: Current distribution and anode shape

J. ZORIC, I. ROUŠAR

Institute of Chemical Technology, Department of Inorganic Technology, 166 28 Prague 6, Czech Republic

J. THONSTAD

Norwegian Institute of Technology, Department of Electrochemistry, N-7034, Trondheim, Norway

Received 15 July 1996; revised 21 October 1996

In aluminium electrolysis cells with prebaked anodes the anode shape changes with time after a new anode has been set, reaching a steady state profile after several days. Mathematical modelling of the anode consumption, using current densities obtained by solving the Laplace equation in 2D space, showed that a constant shape is reached after 6–8.6 days, depending on the width of the gap to a neighbouring anode or to the sidewall of the cell and on the shape of the frozen sideledge. The calculated steady state shapes were similar to measured shapes of industrial anodes. The current density decreases along the side of the anode from the nominal value at the underside (0.75 A cm^{-2}) to a minimum near the surface of the electrolyte (0.08–0.28 A cm^{-2}) depending on the geometry. The fraction of the current passing through the sides of the anode is of the order of 15%. Two approaches to the calculation of the anode shape are discussed: one method of incremental time steps, and one method using the 'near steady-state shape' condition.

List of symbols

a, b	Tafel coefficients for the anodic overvoltage in Equation 2 (V and V decade^{-1})
A	anode cross section area in the x-z plane in Equation A1 (m^2),
C	anode cross-section circumference in the x-z plane in Equation A1 (m),
E	electrode potential (V)
F	Faraday's constant
h	immersion depth of the anode (cm), see Fig. 9
I	current (A)
j	current density (A cm^{-2})
L	length of the anode (cm), see Fig. 9
M	molar mass of carbon in Equation 7 (g mol^{-1})
n	number of electrons in Reaction 1 (n = 4),
r	ratio of the current going through the side of the anode to the total anodic current, see Equation 24
s	length of the anode surface contour (cm), see Fig. 2
t	time (s)
u	the distance ($x_G - x_A$) for a steady state anode profile in Equation 28 (cm), see Fig. 9
U	cell voltage (V)
v	anode movement relative to the coordinate system (cm s^{-1})
w	width of the anode (cm), see Fig. 9
x, y	distances in the x or y directions, respectively (cm)
z_z	unit length in the z direction given in Equation 21 (cm)

Greek symbols

α	angle in Equations 5 and 6 (see Fig. 2)
β	angle (see Fig. 2)
η	overvoltage (V)
η_1	anodic (carbon) consumption with respect to Faraday's law in Equation 7
φ	Galvani potential (V)
ρ	specific resistivity (Ω cm)
ρ^*	density of carbon (g cm^{-3})

Subscripts

A	anode
C	cathode
E	electrolyte
n	value orthogonal to the surface
x	value in the x-direction, x component
y	value in the y-direction, y component
b	value for the flat, bottom part of the anode
rev	reversible,

Superscripts

S	steady state in Equations 18 and 19
k	kth iteration.

0021-891X

1. Introduction

In industrial aluminium cells equipped with prebaked anodes (Fig. 1), a number of baked carbon anodes are positioned parallel to the horizontal aluminium pad, which acts as the cathode. Liquid aluminium is deposited at the cathode and CO_2 is evolved from the anode, which is consumed at a rate of about 1.5 cm per day. The primary cell reaction is

$$2/3\ Al_2O_3 + C = 4/3\ Al + CO_2 \qquad (1)$$

the electrolyte being a fluoride melt (Na_3AlF_6–AlF_3–CaF_2) acting as solvent for alumina. Most of the current passes between the cathode and the horizontal part of the anode facing the cathode, but some current also passes through the vertical sides of the anode. When a new anode is set, the corners become rounded fairly quickly, and this effect is important in facilitating the escape of gas from the underside of the anode.

The current at the sides of the anode affects the current distribution on the cathode, especially in the wide central channel and in the peripheral channel between anodes and sidelining. This current distribution is believed to be of importance for the current efficiency of the process [1]. Current density gradients at the cathode sets up gradients in interfacial tension leading to a Maragoni movement of the interfacial layer [2]. A proper knowledge of the current distribution is also important in cell design and for estimation of the anode–cathode distance, based on the ohmic drop in the electrolyte. It has been claimed that excess anode consumption due to detachment of carbon particles from the anode (so-called carbon dust) predominates at the sides of the anodes where the current density is low [3]. If this effect is to be estimated the current distribution must be known.

The objectives of the present work were to study the current distribution on prebaked anodes, to determine how long it takes to establish a constant shape of the anode side and to compare that shape with measurements, and to calculate how large a fraction of the current passes through the sides of the anodes, depending on the width of the gap between two adjacent anodes and between anode and sidewall. Profiles of anode contours of prebaked anodes used in industrial aluminium cells were measured after the anodes had been taken out of cells, and these shapes were compared with the calculated shapes.

Different methods of studying current distribution in electrochemistry are reported in the literature. Some work [5–15] related to aluminium cells will be reported here. Haupin [4] used a scanning reference electrode to map the equipotential lines and he derived 'fanning factors'. Similar measurements were later made by Kuang and Thonstad [5] on Søderberg cells (with selfbaking anodes). Kulkov and Grinberg [6] proposed the use of physical models to simulate aluminium cells and study the electrical field. Development of powerful computer hardware and software allows numerical modelling and simulations for analysis and cell design. Several workers have performed calculations of the electrical field in different parts of the cell, such as in the anode [13], calculations of cathodic currents [8], anode current density distribution in cells with sloping electrodes [9], and current distribution in the bus bar system [10]. Calculations of the electrical field in 2D cross sections of the cell have been conducted [11–14], for which some authors [1, 11] calculated the primary current distribution and others [12, 13, 14] used the secondary current distribution. Different methods were applied, for example, the finite difference method [7, 13, 14], the finite element and the finite volume methods [11, 12, 14, 15]. Depending on the complexity of the problem and the available soft-

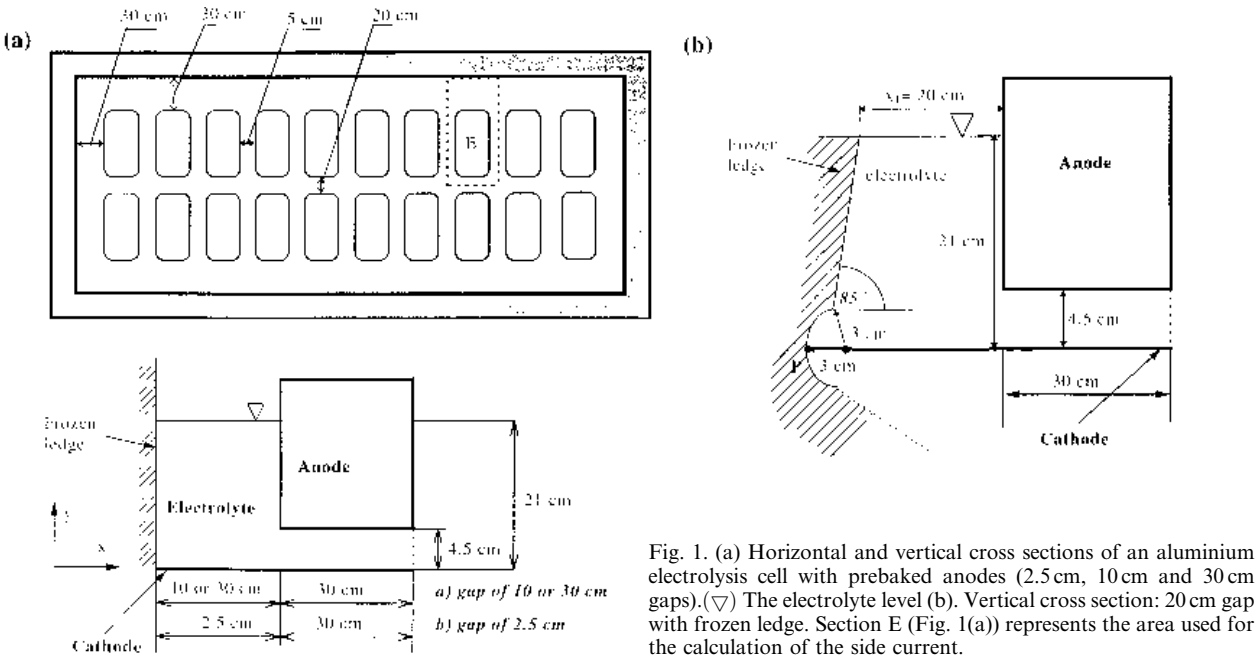

Fig. 1. (a) Horizontal and vertical cross sections of an aluminium electrolysis cell with prebaked anodes (2.5 cm, 10 cm and 30 cm gaps).($\triangledown$) The electrolyte level (b). Vertical cross section: 20 cm gap with frozen ledge. Section E (Fig. 1(a)) represents the area used for the calculation of the side current.

ware, different solutions were used: commercially available software (FIDAP®, PHOENIX/ESTER®, ANSYS®, ABAQUS®, NASTRAN®, ASKA®, etc.), in-house software [15] developed by investigators dealing with modelling, or a combination of these two. Some authors used integrated software solution [16] for multipurpose analysis (magnetohydrodynamics, temperature–electrical fields, magnetic field, stress analysis etc.).

In the present work we focus on the current distribution in the electrolyte of aluminium cells. Possible approaches to the calculation of current distribution are: (i) The use of software for electrical field calculations with developed routines for introducing the electrode polarization, (ii) the use of the identity between the electrical field and the temperature field (approximating the polarization step in the potential at the interface between two materials by the heat transfer resistance, for example using the software FIDAP®).

In [14] and in the present work we used a mesh generator of the commercial software COSMOS® and a solver developed by the authors. A limited number of cases were selected, and a number of simplifying assumptions made. The current density (c.d.) on the side of the anode depends above all on the width of the space the current passes through in the gap facing a neighbouring anode or the sidewall of the cell. Three cases were chosen with the following widths: 2.5 cm, 10 cm and 30 cm. The first corresponds to the narrow 5 cm gap between adjacent anodes, the second corresponds to a 20 cm wide central channel and the last to a 30 cm wide peripheral channel. The sidewall is normally covered by a ledge of frozen electrolyte (cryolite) [17]. Therefore, one case was chosen with a realistic shape of the ledge, as shown in Fig. 1(b) (this is denoted the 20 cm gap with frozen ledge). In the case of a 30 cm gap and a vertical wall (Fig. 1(a)) the wall was considered to be electrically insulating (e.g. covered by a thin ledge). Different ledge shapes and also the case of a conducting sidewall will be treated in a subsequent paper (Part II).

When a new, cold anode is set, it is immediately covered with a layer of frozen electrolyte, which slowly melts away during the first 12–18 h [18]. Apparently the sides and the corners first become exposed to molten electrolyte and start to draw current, while the central part of the underside becomes clear several hours later [18]. Also, because of the horizontal configuration with sharp corners, the underside tends to be blocked by gas bubbles until the corners are rounded off and a gas-induced electrolyte circulation is established. However, model experiments have shown that an inclination of as little as 0.3° is sufficient to set gas bubbles in motion [19].

In the present work the irregular current distribution during the heating-up period was neglected, and time zero was taken as a situation when the entire anode was heated and cleared of frozen electrolyte, so that electrolysis began simultaneously across the entire exposed surface. Any possible effects of waves at the metal–electrolyte interface were also neglected.

2. Theory

To check the influence of the electrical field and the cell geometry on the steady state shape of the anode, the local carbon consumption was calculated. A 2D vertical cross section of a commercial cell was considered, and the electrical field in the cell was calculated under steady state conditions. The overvoltages for both anode and cathode were introduced. The initial shape of the anode was rectangular. The vertical 2D cross sections represent planes located at the centres of the sides of a prebaked anode in the cell (for illustration, see Fig. 1(a)). As already mentioned three different gaps were considered: (i) 30 cm, (ii) 10 cm and (iii) 2.5 cm, and one case with a 20 cm gap with a frozen ledge, as shown in Fig. 1(b). The thinning of the ledge near the metal surface is due to higher heat transfer coefficient in that area. Owing to the geometrical symmetry between two anodes, the central boundary plane can be considered as an insulating plane, so that the calculations carried out also represent the cases when the distances between two anodes are 60 cm, 20 cm and 5 cm, respectively.

Based on Faraday's law, taking the overconsumption (η_I) into account, two methods of calculating the anode consumption were tested. For both methods it was necessary to calculate the electrical field taking into account the anodic and cathodic overvoltages [20, 21]. Steady state conditions were assumed, and any influence on the electrical field of the presence of gas bubbles, the temperature field and the magnetic field was neglected. The presence of gas bubbles known to cause an increased electrolyte ohmic resistance, produces an extra voltage drop of 0.15–0.35 V [4], but it is believed not to affect the current distribution significantly. To calculate the current densities needed for the consumption algorithm, the Laplace equation (LE) for the Galvani potential in 2D was solved [22].

3. Assumptions for solution of the LE in the interelectrode space

The LE in the interelectrode space was solved using the finite element method (FEM) with triangular elements. The following conditions were applied:

(i) Secondary current distribution was considered on both anode and cathode. For the anode the following equation was used:

$$E_A = |E_{rev,\,cell}| + a + b\ \log\ (j_{n,A}) \qquad (2)$$

where $j_{n,A}$ is in A cm^{-2}, $a = 0.5$ V and $b = 0.25$ V decade^{-1}, $|E_{rev,\,cell}| = 1.23$ V [21], valid for Reaction 1 for the following electrolyte compositions: 11 wt % AlF_3, 5 wt % CaF_2, 3 wt % Al_2O_3, balance Na_3AlF_6, all at 960°C.

$$|E_{rev,\,cell}| = E_{rev,\,A} \qquad (3)$$

where the potential is referred to the aluminium electrode. To create the boundary conditions it was assumed that the equipotential line with the potential U_{cell} follows the anode boundary surface from the anode side. Because the electrical conductivity of the carbon anode is about 100 times higher than that of the electrolyte, the anode surface was treated as being equipotential.

(ii) For the cathodic overvoltage a linear polarization curve was assumed [1], and

$$E_C = -0.08 \times |j_{n,C}| \quad (4)$$

The initial shape of the anode was rectangular, as shown in Fig. 1(a). For the solution of the LE a uniform resistivity of 0.465 Ω cm [23] was assumed in the entire electrolyte. In reality areas where there is a mixture of electrolyte and gas bubbles have somewhat higher resistivity. The extra ohmic drop in the electrolyte due to the presence of gas bubbles is in the range 0.15–0.35 V [4].

(iii) To simplify the presentation of the results, the border between the side and the underside of the anode was defined as shown in Fig. 2. The side of the anode is the part of the anode curve going from the surface of the electrolyte, point A to point G. The line going from point G to the orthogonal projection of the vertical side of the anode intercept at an angle β of 45° with the horizontal line representing the flat part of the anode. According to this definition the underside of the anode begins at point G and covers the flat bottom part of the anode, the working face of the anode, that is, in this case up to point K. The length of the anode boundary (s) is then calculated from point A ($s = 0$) through points G, H and up to K.

(iv) The origin of the coordinate system was chosen so that $y = 0$ for the metal surface at any time, and the coordinate origin was located in the left hand side of the cross section under consideration (point O in Fig. 2). With this definition of the coordinate system, a simple form of the formulae was obtained, to facilitate the programming. With such a coordinate system and a constant average current density (nominal cd) on the underside of the anode, no net movement of the anode contour could be assumed at steady state. In reality the cathode surface moves relative to a fixed point on the cell, as metal accumulates. The metal is tapped (every day or every second day), so that there is a sudden drop in the metal level, and the position of the anodes is lowered accordingly. Between tappings the anode does not show very much net movement, because the rise in the metal level only slightly exceeds the anode consumption. However, the anode is subjected to small movements up and down in order to maintain constant cell voltage as part of the computer-based cell control system.

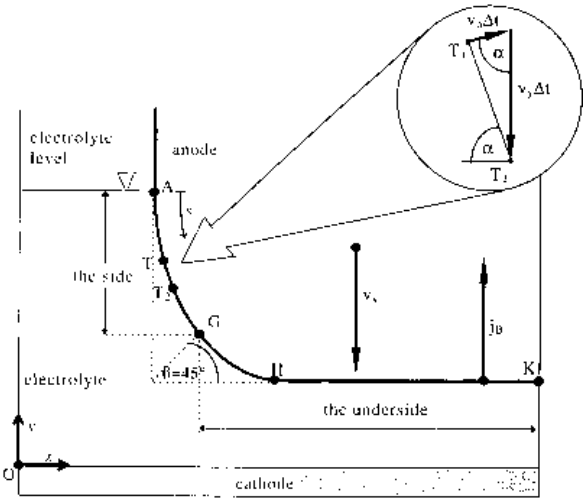

Fig. 2. Schematic cross section of a prebaked anode, with vectors of current densities and velocities illustrating the method of small time steps. The side and the underside of the anode are also defined: j_b current density on the flat part of the anode; j_n, current density on the side of the anode; v_y, velocity of the anode in the y-direction (cm s^{-1}) with respect to the coordinate system.

(v) Owing to variations in temperature and electrolyte composition the thickness of the ledge of frozen electrolyte, shown in Fig. 1(b), varies. The position of the intercept between electrolyte, aluminium and ledge (point P in Fig. 1(b)) is shifted during electrolysis. The shape of the ledge, as well as the position of point P, influence the anode current distribution. The particular case illustrated in Fig. 1(b) was considered in this work.

(vi) The effects of gas bubbles on the electrolyte resitivity and in screening the anode surface were neglected.

(vii) A 150 kA cell having 20 anodes (135 × 75 cm) was considered, and the depth of immersion of the anodes in the electrolyte was 16.5 cm. For other dimensions, see Fig. 1(a) and 1(b). It was assumed that all anodes draw the same current. The c.d. at the underside of the anode was taken to be 0.75 A cm^{-2}, and after simulation for all iterations the side current was calculated.

(viii) To simulate the anode consumption a 15% overconsumption with respect to Faraday's law was assumed, using a factor $\eta_I = 1.15$ (i.e. the anode consumption was calculated as $1.15j/4F$ mol s^{-1}). The overconsumption is caused by dusting and the Boudouard reaction [21]:

$$CO_2 + C \rightarrow 2CO$$

The consumption rate of the anode for a nominal current density of 0.75 A cm^{-2} and an anode density of 1.55 g cm^{-3} was then 1.48 cm per day.

(xi) To abbreviate the subscripts for the anodic c.d., $j_{n,A,}$ only j_n will be used and similarly the c.d. at the flat bottom part of the anode, $j_{n,A,b}$, will be replaced by j_b.

4. Time shifts of the anode contour

The method of small time increments is frequently used to calculate the anode shape in electrochemical machining [24]. Another concept denoted the 'near steady-state shape' condition was developed for the purpose of this study.

4.1. *The method of incremental time steps*

The shifts of the anode contour with time were calculated using the above mentioned assumptions. After every iteration, that is, calculation of the LE for the interelectrode space with the given boundary conditions, the anode consumption was calculated using Faraday's law for Reaction 2. The shifts of the anode boundary points (see Figs 1 and 2) in the x and y directions [22, 24], are described by Equations 5 and 6, respectively. From Fig. 2 it can also be derived that the consumption varies with $\sin\alpha$ in the horizontal direction and with $\cos\alpha$ in the vertical direction:

$$\Delta y = -\left(v_y - k j_n \cos\alpha\right)\Delta t \tag{5}$$

$$\Delta x = -(k j_n \sin\alpha)\Delta t \tag{6}$$

$$k = \frac{\eta_I\, M}{n\ \rho^*\ F} \tag{7}$$

As can be seen from Equations 5 and 6 (before steady state is reached) each node located on the anode boundary has to be moved in the x and y directions, respectively, for the increments Δx and Δy after the time increment Δt. There are several ways to calculate the new positions of the points and to obtain a smooth anode shape. Since the magnitudes of the shifts are different for different elements, it has to be decided where the new nodes should lie. Two possible techniques were considered for the calculation of the positions of the new nodes:

(a) New nodes can be placed on orthogonals passing through the nodes of the previous curve/surface (as shown in Fig. 42.9.6 in [22]). In this case the shifted sides of the triangles are no longer parallel to the previous ones. This geometrical construction has the disadvantage that the calculated consumption of anode material is not in perfect agreement with Faraday's law (neither for the elements nor for their sums) [22].

(b) To eliminate this error, new nodes can be placed on the orthogonals to the surface passing through the nodes of the previous curve/surface, and in this way the condition for the local consumption of the anode satisfies Faraday's law. (For more details see Figs 42.9.5 and 42.9.6 and chapter 42.9 in [22].) In the present work method (b) for the shift of the anode boundary was used.

4.2. *Method of the 'near steady state shape' condition*

The calculation of the changing coordinates of the anode surface during the passage of current is based on Faraday's law. From Faraday's law the rate of the shift of the anode surface (v_n) in the direction orthogonal to the surface is given by

$$v_n = k \times j_n \tag{8a}$$

It is assumed that k is independent of the current density (η_I is constant). The movement of the anode (i.e. the anode movement orthogonal to the cathode surface relative to the coordinate system) satisfies the condition given by the equation:

$$v_y = k \times j_b \tag{8b}$$

Describing the anode contour as $G(x)$, that is, as a function of the coordinate x, we have

$$G'(x) = \frac{\mathrm{d}G(x)}{\mathrm{d}x} \tag{9}$$

and also

$$G'(x) = -\tan(\alpha) \tag{10}$$

where α is a function of x.

By means of Equation 10 the shifts $(\Delta x, \Delta y)$ of the anode contour along the coordinate axes during a time interval Δt can be expressed (vol 1, page 110 of [22]) as

$$\Delta y = -[v_y - v_n \cos\alpha]\Delta t \tag{11}$$

$$\Delta x = v_n \sin\alpha\, \Delta t \tag{12}$$

The velocity v_y is the shift of the anode in the y direction (in the side section of the anode) relative to the coordinate system. For the coordinate system and the orientation of the shifts, see Figs 1(a) and 2.

Equations 11 and 12 denote the technique of moving boundary points mentioned in the previous chapter. These increments (Δx and Δy) are added to the coordinates of the nodes at the anode surface to obtain the new coordinates:

$$y_i^{k+1} = y_i^k + \Delta y(i,j) \tag{13}$$

$$x_i^{k+1} = x_i^k + \Delta x(i,j) \tag{14}$$

Equations 11 and 12 involve the rate component v_y, expressing the rate of the shift of the anode with respect to the cathode surface. As pointed out above, the cathode surface (i.e. the surface of the aluminium pool) is regarded as motionless, serving as the origin of the coordinate system. Equations 13 and 14 are used for the calculation of the new coordinates of the nodes on the anode surface, which gives the new contour $y = G(x)^{k+1}$; and by differentiation, its derivative $G'(x)^{k+1}$. The procedure described by Equations 11 to 14 should give the steady state anode contour after a sufficient number of Δt steps.

The steady state contour $G^S(x)$, can be obtained by the elimination of Δt from Equations 11 and 12 and by replacing $\Delta y/\Delta x$ by $-\tan\alpha$.

$$\tan\alpha = \frac{v_y - v_n \cos\alpha}{v_n \sin\alpha} \tag{15}$$

giving the 'cosine rule' [24]:

$$\cos\alpha = v_n / v_y = j_n / j_b \tag{16}$$

which states that the rate of consumption of the curved part of the anode relates to the vertical consumption rate as $\cos\alpha$.

Using Equation 10 we obtain

$$G'(x) = \frac{dy}{dx} = -\left[(v_y/v_n)^2 - 1\right]^{1/2} \quad (17)$$

After rearrangement of Equation 17 and integration from x_1 to x_2, it follows that

$$G^S(x_2) = G^S(x_1) - \int_{x_1}^{x_2} \left[\left(v_y^S/v_n^S\right)^2 - 1\right]^{1/2} dx \quad (18)$$

Instead of calculating the value of the coordinate y of the steady state curve, $G^S(x)$, it may, in some cases, be more convenient to calculate the coordinate x of the $G^S(x)$. Equation 17 may be rearranged and integrated from y_1 to y_2 :

$$x_2^S = x_1^S + \int_{y_1}^{y_2} \left[\left(v_y^S/v_n^S\right)^2 - 1\right]^{-1/2} dy \quad (19)$$

Equation 19 allows the calculation of the steady state coordinate x for the steady state anode profile. The use of Equation 18 can be recommended for those parts of the $G(x)$ curve where the changes in the x direction prevail over the changes in the y direction, while Equation 19 can be recommended for the opposite case.

The steady state shape of the anode is related to the local current densities, (see Equations 18 and 19), because v_n is calculated from Equation 8(a). It should be noted, that $|v_y| \geq v_n$ at steady state along the anode contour. The opposite case of $|v_y| < v_n$ cannot exist at steady state; that is, the current densities at the anode side (j_n) cannot be higher than at the bottom part (j_b). This also follows from the cosine rule (Equation 16).

It should be emphasized that Equations 18 or 19 and the solution of the LE, which gives the local c.d.s, should be calculated as many times as necessary until the coordinates of the anode points do not change significantly. The use of these equations is a reasonable method for the calculation of the near steady state anode shape $G^S(x)$. The number of solutions of the LE is reduced dramatically compared with calculation of the new anode shapes for incremental Δt steps by means of Equations 5 and 6. Tests showed that with the first method 10 iterations were needed with Δt steps equal to 12 h, and 5–6 additional iterations with steps of 4 h, representing 15–16 solutions of the LE for the interelectrode space. With the second method it was sufficient to calculate the LE and Equations 18 or 19 four to five times only to reach the 'near steady-state anode shapes'. The method of small Δt steps is influenced by the 'bad' elements (far from an equilateral triangle) in the mesh to a greater extent than the method of 'the near steady-state condition'. But the method of 'the near steady-state condition' cannot be used for those parts of the anode where the current density is higher than j_b. In such regions all higher c.d.s are replaced by j_b. Therefore, this method is not so precise near the anode corner where calculated c.d.s are often higher than j_b. This method gives the anode boundary curves at several discrete times, say $\Delta t_1, \Delta t_2, \Delta t_3$. Any interpolation should be based on Equations 5 and 6. Usually v_y is calculated for the underside of the anode, with the c.d. j_b.

By mathematical analysis of Equations 18 and 19 it can be concluded that the anode contour $G^s(x)$ can have maxima and minima. Current densities at all points located at $G^s(x)$, which fulfill the condition $G^s(x)'' = 0$ are equal to j_b. No local c.d. can be higher than j_b for the steady state anode contour. From Equation 15 the cosine rule (i.e. Equation 16) is obtained, where α is the angle to the horizontal, calculated for any point located at $G^s(x)$.

Equations 18 and 19 allow the calculation of the 'near steady-state anode shape' $G^s(x)$ from the local c.d.s. Estimation of the time between two successive anode shapes can be based on Equations 11 and 12 with an accuracy of 20%. The LE solved for the Galvani potentials located in the interelectrode space of the cell with the given (or assumed) 'near steady-state anode shape' gives the local c.d.s along the anode surface as one of the results. This means that the LE and Equations 18 and 19 should be satisfied at the same time for the steady state anode contour.

5. Results and discussion

5.1. *Anodic current distribution*

The steady state anode contours of a prebaked anode were calculated starting with the initial rectangular shape shown in Fig. 1(a) and (b). Equipotential lines in the interelectrode space, for the steady state shapes of the three cases denoted as 2.5 cm gap, 10 cm gap and 30 cm gap are shown in Fig. 3(a)–(c), respectively. The thick lines in Fig. 3(b) and (c) represent the equipotential lines at the potential 1.8 V. These lines follow closely the shape of the anode boundary. However in Fig. 3(a) the thick line is not the equipotential line at 1.8 V, but the line of the anode boundary. The equipotential line of 1.8 V is identical with the anode boundary line at the lower part of the anode boundary. At the side of the anode the 1.8 V equipotential line crosses the space ending at the insulating wall. This is caused by the low c.d. (low potential) in that area. To visualize the potential field distribution 3D figures are presented in the upper right corner of all three graphs.

Anode shapes close to steady state were obtained after six days of electrolysis (simulation) for the 2.5 cm gap, after 8.6 days for the 10 and 30 cm gaps and 20 cm gap with frozen ledge (Fig. 1(b)). In Fig. 4 the c.d.s for all the calculated cases (and for their iterations expressed in days) are shown. The length of the anode boundary (depicted as s in Fig. 2) was taken as the abscissa, representing the physical length

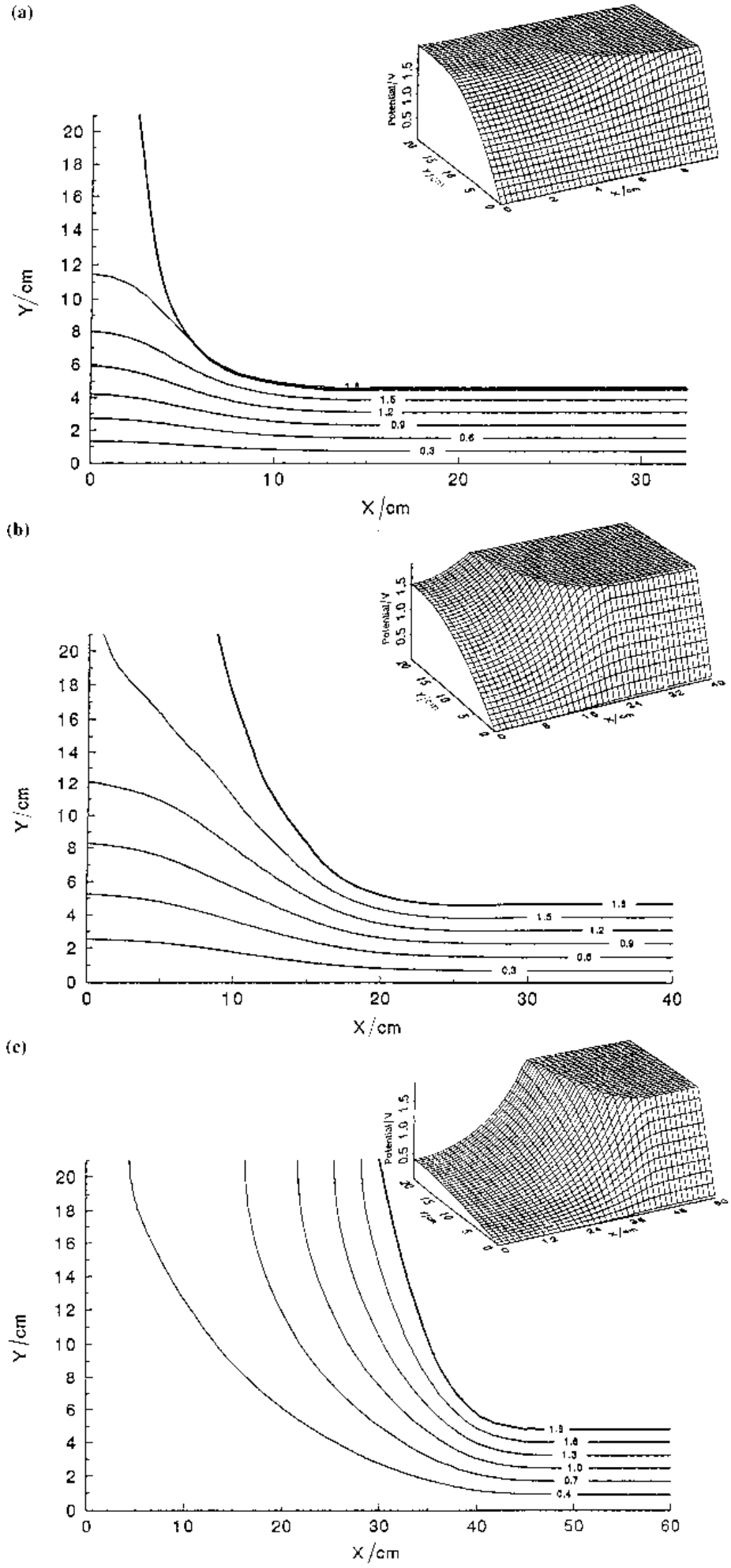
(a)
Potential/V
0.5 1.0 1.5
Y/cm
X/cm
1.8
1.5
1.2
0.9
0.6
0.3
(b)
Potential/V
0.5 1.0 1.5
Y/cm
X/cm
1.8
1.5
1.2
0.9
0.6
0.3
(c)
Potential/V
0.5 1.0 1.5
Y/cm
X/cm
1.9
1.6
1.3
1.0
0.7
0.4

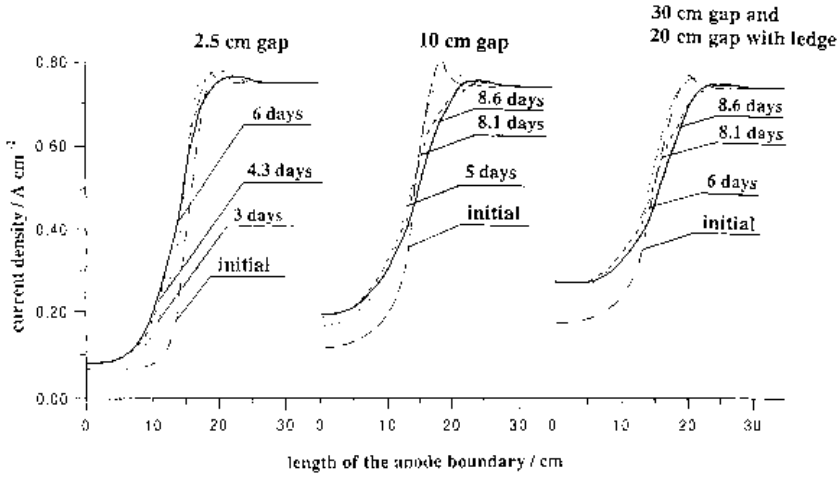

Fig. 4. Local current densities on the surface for an anode with three different gaps (2.5 cm, 10 cm, 30 cm and 20 cm with ledge) from left to right. The length of the anode boundary is calculated from the electrolyte level $s = 0$ along the side of the anode.

of the boundary going from the uppermost anode boundary point (point A in Fig. 2) to the underside of the anode (5 cm to the right of point H in Fig. 2). Beyond that point the c.d. has a constant value of 0.75 A cm^{-2} in all cases. To see the local c.d. as a function of the coordinates x and y, respectively, Figs 5–9 may also be analysed.

At the corner of the anode the shape was not stable during the mathematical simulation. A local maximum in the c.d. was obtained, as can be seen from Fig. 4, and during the time of electrolysis (simulation) this maximum moved over a range of approximately 5 cm in the x direction. The maximum c.d. was from 1 to 10% higher than j_b. The maxima in these calculations are due to 'the geometrical approximation', caused by the rough division of the anode contour and the shape of the triangles around it. The anode contour was approximated by straight lines of approximately 3 mm length. The uncertainty of the calculated steady state anode shape is 0.1–2 mm in the x direction. This means that small changes of the anode shape may lead to more pronounced changes of the local c.d. and to corresponding shifts in the calculated anode shape in this region.

In Figs 4 and 5 the results of the calculation for an anode with a 2.5 cm gap are shown. Figure 5 shows anode shapes for different durations of electrolysis and also the shape which was found experimentally. After three iterations (representing 6 days) the resulting shape stopped changing significantly. The agreement between the measured and the calculated steady state shapes is very good.

Figure 6 presents the development of anode shapes for a 10 cm gap. After 4 iterations (representing 8.6 days) a steady state anode shape was obtained. For the 10 cm gap also a small deviation exists between the calculated and the measured anode shape.

Figure 7 shows the development of anode shapes for 30 cm and 20 cm gaps with ledge (Fig. 1(b)). The steady state shape was obtained after 8.6 days. The difference in c.d. between the 30 cm gap (with the sideledge orthogonal to the cathode) and 20 cm gap with ledge (with an angle of 85° between the sideledge and the cathode) is less than 5%. More information about the influence of the sideledge on the current distribution is presented in Part II [25].

A comparison of all the calculated steady state shapes is shown in Fig. 8. It can be seen that the width of the gap has a marked influence on the shape of the anode.

5.2. *Current passing through the side of the anode for different cross sections*

To obtain the current passing through the side of the anode for a 2D cross section, the integral of the c.d. along the surface of the anode was calculated, using the following formulae, where the subscripts refer to Fig. 2.

$$I_{AK} = I_{AG} + I_{GK} \tag{20}$$

$$I_{AG} = z_z \int_A^G j_n \mathrm{d}s \tag{21}$$

$$I_{GK} = z_z \int_G^H j_n \mathrm{d}s + z_z \int_H^K j_b \mathrm{d}s \tag{22}$$

where s is the boundary line of the anode and z_z is the unit length in the z direction. The positions of the points A, G, H and K on the anode boundary are shown in Fig. 2. The length of the anode boundary s is related to x by the equation,

$$\mathrm{d}s = \mathrm{d}x / \cos\alpha \tag{23}$$

Fig. 3. Equipotential lines (in V) in the interelectrode space, for the steady state anode shape. Origin of the coordinate system is at the left bottom corner of the graph. Figures in the left upper corner represent a 3D presentation of the electrical field. (a) 2.5 cm gap (distance between the insulating wall and anode is 2.5 cm), (b) 10 cm gap, (c) 30 cm gap.

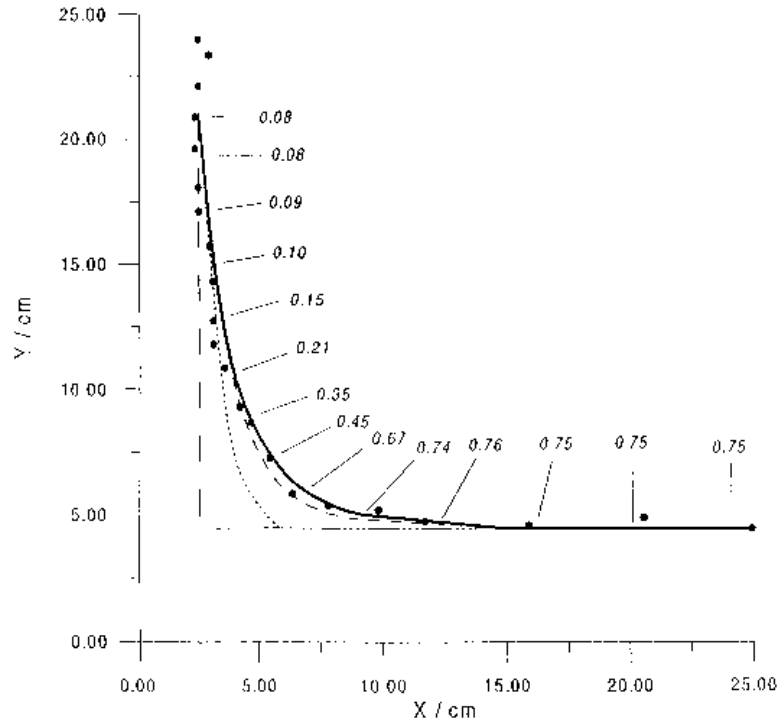

Fig. 5. Changes of anode shape with 2.5 cm gap. The numbers represent the local c.d. (in A cm^{-2}) along the anode shape at steady state. Key: (●) measured shape at steady state; (— —) initial shape; (- - - -) after 3 days of electrolysis; (– – –) after 4.3 days of electrolysis; (———) after 6 days of electrolysis.

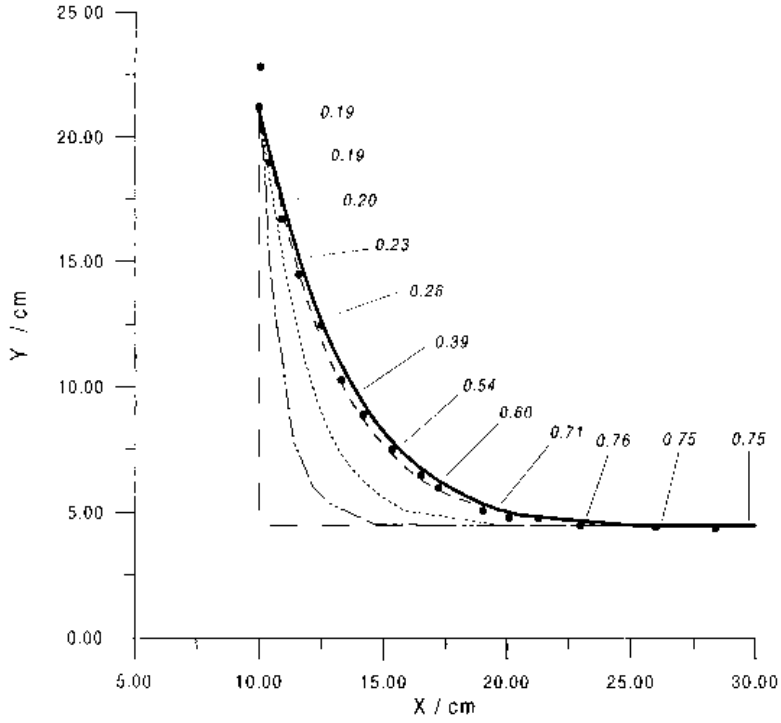

Fig. 6. Changes of anode shape with 10 cm gap. The numbers represent the local c.d. (in A cm^{-2}) along the anode shape at steady state. Key: (●) measured shape at steady state for an anode facing the central channel; (— —) initial anode shape; (– ·· — ·· — ·· –) after 3 days of electrolysis; (- - - - -) after 5 days; (– – – – –) after 8.1 days; (———) after 8.6 days.

The ratio of the current through the side of the anode (2D cross-section) to the total current is given by the following equation:

$$r = I_{AG}/I_{AK} \tag{24}$$

The current per unit length in the z direction passing through the side of an anode (see Fig. 1(b)) facing a 2.5 cm gap is 2.24 A cm^{-1} and the same current for a 10 (30) cm gap is 3.22 (3.78) A cm^{-1}.

Estimation of the current passing through the side of the anode was also made by Haupin [4]. Haupin calculated 'fanning factors', symbolizing the current that fans out from the side of the anode. It is not equivalent to the side current calculated in the present

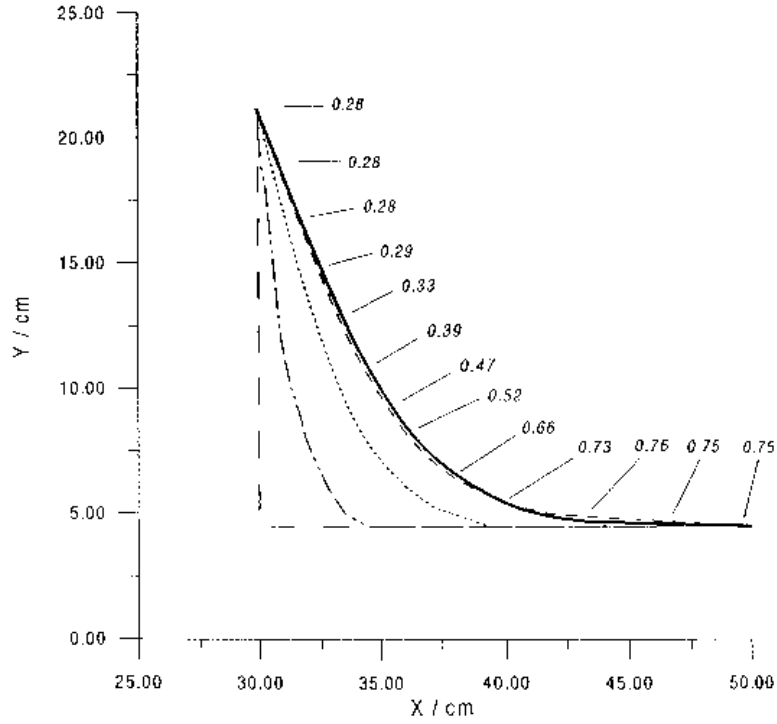

Fig. 7. Changes of anode shape with 30 cm gap and 20 cm gap with ledge as well. The numbers represent the local c.d. (in A cm^{-2}) along the steady state anode shape. Key: (— —) initial shape; (– – – –) after 3 days of electrolysis; (- - - - - -) after 6 days; (– – – – –) after 8.1 days; (———) after 8.6 days.

work, but it has a similar significance. For instance, for a 25 cm distance to a neighbouring anode, 4.5 cm interpolar distance and 15–18 cm electrolyte depth the fanning factor is 5.7 cm [4]. For a nominal current density of 0.75 A cm^{-2} this corresponds to a current per unit length of 4.3 A cm^{-1}. This corresponds to our value for 30 cm gap of 3.78 A cm^{-1}. The difference can be partly ascribed to the way we define the anode side, that is from A to G in Fig. 2.

At steady state $\cos\alpha$ is defined by Equation 16. By introducing I_{AG} (see Fig. 2) as

$$I_{AG} = z_z \int_A^G j_n / \cos\alpha \, dx \tag{25}$$

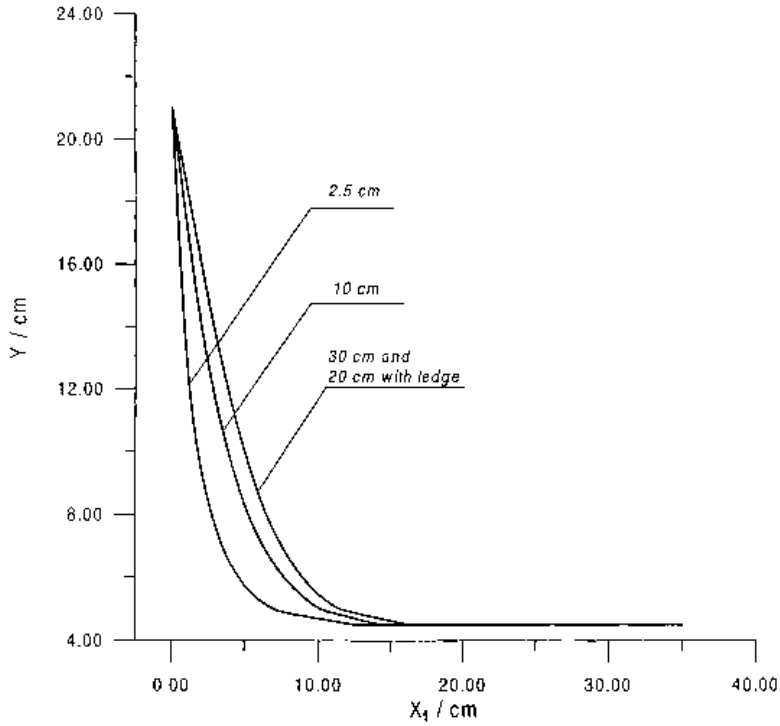

Fig. 8. Comparison of the steady state anode shapes for different gaps as indicated on the figure. x_1 represents the horizontal distance ($x - x_A$), where the point A is given in Fig. 2. y is the coordinate defined in Fig. 2.

and using Equation 16, we obtain:

$$I_{AG} = j_b z_z (x_G - x_A) \tag{26}$$

This is equivalent to the statement that after reaching steady state the averaged current density for the side of the anode calculated on the orthogonal projection of the anode $(x_G - x_A)$ is equal to the current density at the horizontal part of the anode. Similarly it follows that $I_{AK} = j_b z_z (x_K - x_A)$. By means of Equation 26 the ratio r (Equation 24) can be written for the steady state shape of the anode (2D) as

$$r = \frac{x_G - x_A}{x_K - x_A} \tag{27}$$

5.3. *Current passing through the sides of the anode at steady state (in 3D)*

Two methods for the estimation of the current passing through the sides of the anode (in 3D) will be presented, using the results of the 2D calculations given above.

(i) To illustrate the first method one example will be calculated for an anode with dimensions 135×75 cm drawing a current of 7500 A. To calculate the side current passing through the anode (in 3D) the side currents (per cm) calculated from the above mentioned 2D cross sections will be used. For the 2D calculations of the current density distribution along the anode the current passing through the side of the anode is integrated by Equation 21. The currents per cm length in the z direction are given above (Section 5.2). For an anode located in zone E in Fig. 1(a) which faces neighbouring anodes on two sides at a length of 135 cm, and a 30 cm and a 10 cm gap on the short sides of 75 cm lengths (disregarding corner effects) the following estimate of the side current can be made: $2.24\,\mathrm{A\,cm^{-1}} \times 2 \times 135\,\mathrm{cm} + (3.78\,\mathrm{A\,cm^{-1}} + 3.22\,\mathrm{A\,cm^{-1}}) \times 75\,\mathrm{cm} = 1130\,\mathrm{A}$ which represents 15% of the total current passing through the anode.

(ii) To develop a general formula for the estimation of the ratio of the current passing through the side of the anode (in 3D) to the total current at steady state, the distance $x_G - x_A$, will be denoted as u as illustrated in Fig. 9 (Equation 26). Because each side of the anode may have different side currents and distances $u \equiv (x_G - x_A)$, the parameters $u_1 - u_4$ are introduced for each side of the anode. In Equation 26 the term $z_z(x_G - x_A)$ is replaced by wu_1, wu_2, $(L - u_1 - u_2)u_3$ and $(L - u_1 - u_2)u_4$, respectively. This approximation of $z_z(x_G - x_A)$ is reasonable because $w \sim L \gg u_1 \sim u_2 \sim u_3 \sim u_4$ (see Fig. 9). Instead of $z_z(x_K - x_A)$ the term wL is used representing the anode cross section.

From Equations 24 and 26, by summing for all sides of the anode, the ratio r of the current going through the sides of the anode to the total current can be expressed as:

$$r = \frac{u_1 w + u_2 w - u_1 u_3 - u_2 u_3 + u_4 L + u_3 L - u_1 u_4 - u_2 u_4}{wL} \tag{28}$$

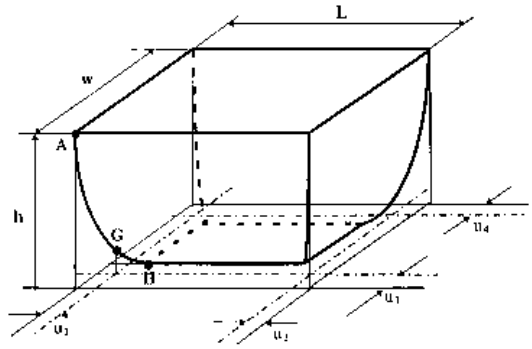

Fig. 9. Schematic of an anode with dimensions and distances necessary for the calculation of the current passing through the anode side (in 3D). See Fig. 2 with 2D cross section of an anode and also Equation 28.

The terms u_1u_3, u_2u_3, u_1u_4 and u_2u_4 are due to overlapping of the strips u_1w, u_2w, u_3L and u_4L at the corners of the anode (Fig. 9). Equation 28 can be rearranged

$$r = \frac{w(u_1 + u_2) + L(u_3 + u_4) - (u_1 + u_2)(u_3 + u_4)}{wL} \tag{29}$$

The values of u, which were evaluated for the calculated steady state shapes of the anode in 2D, for different angles β, are shown in Table 1. Using these values of u, the ratio of the current passing through the side of the anode to the total current (in 3D) can be estimated from Equations 28 or 29.

In Table 2 the ratio of the current through the side of the anode (located in zone E in Fig. 1(a)) to the total anodic current was calculated using Equation 29 for the angle β (Fig. 2) of $45°, 50°, 55°$ and $60°$, respectively. For β of $45°$ $r = 0.149$ (i.e. 14.9%) of the total current passes through the side of the anode, in close agreement with the previous calculation. With increasing angle β the current through the side of the anode falls because the area defined as side area decreases, and for $\beta = 60°$ $r = 0.114$ (i.e. 11.4%).

In Appendix 1 the ratio of the current through the side of the anode to the total current is calculated for Søderberg and prebaked anodes using a simplified equation derived from Equation 29.

5.4. *Cathodic current distribution*

Figure 10 shows the current distribution along the cathode surface for the calculated gaps. When com-

Table 1. Values of $u \equiv (x_G - x_A)$ calculated for the steady state shape of the anode facing 2.5, 10 and 30 cm gaps. See also Figs 1 and 9 and Equations 28 and 29.

	u / cm		
β	*2.5 cm gap*	*10 cm gap*	*30 cm gap*
45°	2.980	4.294	5.037
50°	2.750	4.070	4.800
55°	2.450	3.726	4.500
60°	2.330	3.450	4.112

Immersion depth of the anode into the electrolyte was $h = 16.5$ cm.

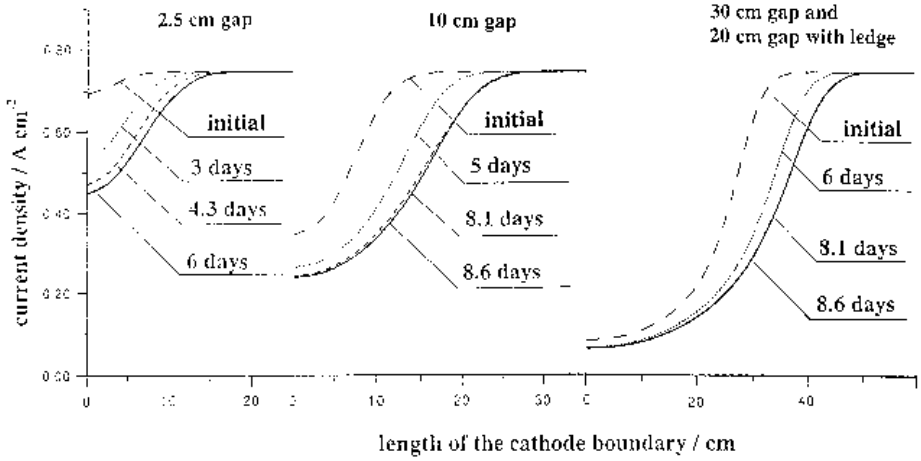

Fig. 10. Local current densities on the surface of the cathode for different gaps (2.5 cm, 10 cm, 30 cm and 20 cm with ledge) from left to right.

Table 2. Ratio of side current to total current for different angles β for an example in which the anode faces a 2.5 cm gap from two long sides (w = 135 cm), from one side (L = 75 cm) a central channel - 10 cm gap and from the other side the ledge with frozen electrolyte - 20 cm gap.

β	I_{side} / I_{total}
45°	0.143
50°	0.134
55°	0.122
60°	0.115

See Equation 29 and zone E in Fig. 1(a)

paring the current distribution along the cathode surface for 2.5 cm, 10 cm and 30 cm gaps, respectively, we note that the wider the gap, the lower the cathodic c.d. in the gap. The current distribution changes during the lifetime of an anode. For all cases the c.d. underneath the working part of the anode was 0.75 A cm^{-2}.

References

[1] P. A. Solli, T. Haarberg, T. Eggen, E. Skybakmoen and A. Sterten, 'Light Metals 1994' (edited by U. Mannweiler), TMS, Warrendale PA, pp. 195–203.
[2] T. Utigard, 'Aluminium 63' (1987), pp. 606–13.
[3] E. R. Cutshall and V. L. Bullough, 'Light Metals 1985' (edited by J. W. Evans), TMS, Warrendale PA, pp. 1039–76.
[4] W. E. Haupin, *J. Metals* **23** (1971) 46.
[5] Z. Kuang and J. Thonstad, *J. Appl. Electrochem.* **26** (1996) 481.
[6] V. N. Kulkov and I. S. Grinberg, 'Light Metals 1996' (edited by W. Hale), TMS, Warrendale PA, pp. 369–74.
[7] A. Piotrowski and S. Pietrzyk, *Metall. & Foundry Eng.* **16** (1990) 315–37.
[8] A. Furman, 'Light Metals 1978', TMS, Warrendale PA, pp. 87–106.
[9] D. Kasherman and M. Skyllas-Kazaros, 'Aluminium 66' (1990), pp. 1157–60.
[10] T. Tvedt and H. G. Nebell, 'Light Metals 1995' (edited by J. Evans), TMS, Warrendale PA, pp. 295–99.
[11] K. J. Fraser, D. Billinghurst, K. L. Chen and J. T. Keniry, 'Light Metals 1989' (edited by P. G. Campbell), TMS, Warrendale PA, pp. 219–26.
[12] D. P. Ziegler, 'Light Metals 1991' (edited by E. L. Rooy), TMS, Warrendale PA, pp. 363–74.
[13] W. W. Hyland, 'Light Metals 1984', TMS, Warrendale PA, pp. 711–20.
[14] J. Zoric, I. Rousar, J. Thonstad and Z. Kuang, to be published in J. Appl. Electrochem.
[15] I. Tabsh and M. Dupuis, 'Light Metals 1995' (edited by J. V. Evans), TMS, Warrendale PA, pp. 295–99.
[16] D. Vogelsang and M. Segatz, 'Light Metals 1991' (edited by E. L. Rooy), TMS, Warrendale PA, pp. 375–78.
[17] K. Grjotheim, B. J. Welch and M. P. Taylor, 'Light Metals 1989' (edited by P. G. Campbell), TMS, Warrendale PA, pp. 255–60.
[18] R. Odegard, A. Solheim and K. Thovsen, 'Light Metals 1992' (edited by E. R. Cutschall), TMS, Warrendale PA, pp. 457–63.
[19] F. N. Ngoya and J. Thonstad, *Electrochem. Acta* **30** (1985) 1659–64.
[20] K. Grjotheim, C. Krohn, M. Malinovsky, K. Matiasovsky and J. Thonstad, 'Aluminium Electrolysis', 2nd edn, Aluminium-Verlag, Dusseldorf (1982).
[21] K. Grjotheim and H. Kvande, 'Introduction to Aluminium Electrolysis', Aluminium-Verlag, Dusseldorf (1993).
[22] I. Rousar, K. Micka and A. Kimla, 'Electrochemical Engineering', Academia, Prague Elsevier, Amsterdam (1986).
[23] J. Hives, J. Thonstad, A. Sterten and P. Fellner, 'Light Metals 1994' (edited by U. Mannweiler), TMS, Warrendale PA, pp. 187–94.
[24] I. Rousar, 'Electrochemical Machining', (in Czech), Institute of Chemical Technology, Prague (1985).
[25] J. Zoric, I. Rousar, T. Haarberg and J. Thonstad, in preparation.

Appendix 1: Difference in the current passing through the side of the anode between Søderberg and prebaked anodes

If Equation 29 is simplified by neglecting the term $(u_1 + u_2)(u_3 + u_4)$ which represents the correction in the geometry at the corners of the anode, and if $u_1 = u_2 = u_3 = u_4$, it follows that

$$\frac{I_{side}}{I_{total}} = \frac{2(w+L)u}{wL} = \frac{Cu}{A} \qquad \text{(A1)}$$

where C is the circumference of the anode and A is the surface of the anode cross section in the $x - z$ plane.

For a Soderberg anode of dimensions 2.8 m × 7.15 m: $A = 20.02\,m^2$, $C = 19.90$ m, $u = 0.04$ m [4] and $I_{side}/I_{total} = 0.04$ (4%)

For a prebaked anode of dimensions 0.75 m × 1.35 m: $A = 1.0125\,m^2$, $C = 4.2$ m, $u = 0.04$ m and $I_{side}/I_{total} = 0.168$ (16.8%)

In this simplified example the current through the sides of the anode for a prebaked anode is 16.8%, that is, four times higher than for a Søderberg anode (4%). The reason for this follows from the geometry, that is, the ratio between the circumference C and the surface area of the anode cross section in the $x - z$ plane denoted as A, see Equation A1.